

Stability of Confined Vortex Sheets

Bartosz Protas

Department of Mathematics and Statistics,
McMaster University, Hamilton, ON, Canada
Email: bprotas@mcmaster.ca

January 8, 2022

Abstract

We propose a simple model for the evolution of an inviscid vortex sheet in a potential flow in a channel with parallel walls. This model is obtained by augmenting the Birkhoff-Rott equation with a potential field representing the effect of the solid boundaries. Analysis of the stability of equilibria corresponding to flat sheets demonstrates that in this new model the growth rates of the unstable modes remain unchanged as compared to the case with no confinement. Thus, in the presence of solid boundaries the equilibrium solution of the Birkhoff-Rott equation retains its extreme form of instability with the growth rates of the unstable modes increasing in proportion to their wavenumbers. This linear stability analysis is complemented with numerical computations performed for the nonlinear problem which show that confinement tends to accelerate the growth of instabilities in the nonlinear regime.

1 Introduction

Shear layers play an important role in fluid mechanics as they appear in many flows of industrial and geophysical significance when boundary layers separate from solid objects. A key property of shear layers is that under typical conditions they are unstable and undergo the Kelvin-Helmholtz instability as a result of which the vorticity from the shear layer rolls up into big vortices. When occurring recurrently, this phenomenon can in turn give rise to a turbulent cascade. In this investigation we are interested in a simple inviscid model of the Kelvin-Helmholtz instability occurring in a channel with solid walls. In the context of more realistic flows this problem was studied using an approach based on the theory of viscous potential flows in [1] where the effect of various problem parameters on the growth rates of unstable modes was analyzed. Analogous questions relevant for the stability of confined jets in circular geometries in the presence of heat and mass transfer were considered in [2].

Inviscid vortex sheets, represented as one-dimensional (1D) curves across which the tangential velocity component exhibits a discontinuity and evolving under their own induction in a potential flow, have been frequently invoked as a mathematical abstraction of actual viscous shear layers [3]. In unbounded domains they admit an elegant description in terms of the Birkhoff-Rott equation. This singular integro-differential equation has a number of interesting properties — in particular, its equilibrium solution representing a flat (undeformed)

vortex sheet is highly unstable to small-wavelength perturbations, a fact that underlies the ill-posedness of the Birkhoff-Rott model [4]. As a result, computational studies involving the Birkhoff-Rott equation typically require some regularization in order to track its long-time evolution, usually in the form of the well-known “vortex-blob” approach [5] or using the more recent Euler-alpha strategy [6]. A generic feature characterizing the evolution of (regularized) inviscid vortex sheets is roll-up producing localized vortex spirals [7]. There are many interesting mathematical questions concerning various aspects of the Birkhoff-Rott equation and we refer the reader to the collection [8] and monograph [9] for further details on this topic. The problem of vortex sheet roll-up was recently revisited in [10]. As was shown in [11], despite the severe instability of the Birkhoff-Rott equation, the equilibrium corresponding to the flat sheet can be efficiently stabilized using methods of modern control theory. We add that inviscid vortex sheets endowed with mass inertia and bending rigidity have been used to model flutter phenomena and results concerning the stability of a flapping flag in a channel were reported in [12].

While the Birkhoff-Rott equation has been originally applied on unbounded or laterally unbounded domains (i.e., domains periodic in the streamwise direction and unbounded in the transverse direction), in this study we consider vortex sheets confined to a *bounded* domain with parallel walls representing a channel. By considering the Birkhoff-Rott equation modified to account for the presence of such solid boundaries, we derive a dynamical system describing the evolution of a confined vortex sheet and demonstrate that, interestingly, confinement does not change the key features of the linear instability of the vortex sheet. More specifically, in the presence of solid boundaries the growth rates of the unstable modes remain unchanged as compared to the original case with no confinement. We note that this particular conclusion can also be deduced as a special limiting case from Rayleigh’s classical stability analysis of parallel flows [13, 14]. Numerical solution of the nonlinear problem indicates that confinement in fact enhances the growth of instabilities in the nonlinear regime. The structure of the paper is as follows: in the next section we first recall the Birkhoff-Rott equation and show how it can be modified to account for the effect of solid boundaries; then, in Section 3 we study the linear stability of the equilibria in the new model, whereas in Section 4 we present results obtained from the numerical solution of the nonlinear problem; some final comments are deferred to Section 5.

2 Inviscid Vortex Sheets

In this section we introduce a model for an inviscid vortex sheet confined in a channel with two parallel walls located symmetrically above and below the sheet in its equilibrium configuration, cf. Figure 1. We assume that the flow is periodic, with period 2π , in the streamwise direction x . As is common in the study of such problems [3], we will extensively use the complex representation of different quantities and will identify a point $(x, y) \in \mathbb{R}^2$ in the 2D space with $z = x + iy \in \mathbb{C}$ in the complex plane, where $i = \sqrt{-1}$ is the imaginary unit. Let then $z(\gamma, t)$ denote the position of a point (in the fixed frame of reference) on the sheet which corresponds to the circulation parameter $\gamma \in [0, 2\pi]$ and some time t . The quantity γ represents a way of parameterizing the sheet and for sheets of constant intensity is proportional to the arc-length of the curve. Periodicity of the sheet then implies

$$z(\gamma + 2\pi, t) = z(\gamma, t) + 2\pi, \quad \gamma \in [0, 2\pi]. \quad (1)$$

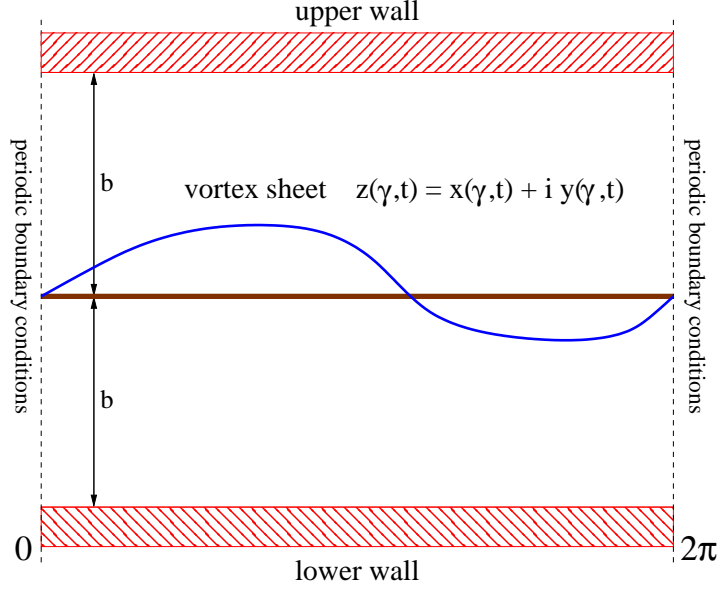


Figure 1: Schematic representation of a confined vortex sheet. The thick brown line represents the equilibrium configuration $\tilde{z}(\gamma)$, $\gamma \in [0, 2\pi]$.

When the sheet is in a laterally unbounded domain, its evolution is governed by the Birkhoff-Rott equation [3]

$$\frac{\partial z^*}{\partial t}(\gamma, t) = V(z(\gamma, t)) := \frac{1}{4\pi i} \text{pv} \int_0^{2\pi} \cot \left(\frac{z(\gamma, t) - z(\gamma', t)}{2} \right) d\gamma', \quad (2)$$

where z^* denotes the complex conjugate of z , the integral on the right-hand side (RHS) is understood in Cauchy's principal-value sense and $V(z) = (u - iv)(z)$ represents the complex velocity at the point z with u and v the horizontal and vertical velocity components (“:=” means “equal to by definition”).

We now consider time evolution of a confined vortex sheet on a domain $\Omega := \{(x, y) : x \text{ is } 2\pi\text{-periodic, } -b < y < b\}$, with straight boundaries $\partial\Omega$ located at $y = \pm b$ for some $b > 0$, cf. Figure 1. Distance b will serve as the main parameter in the problem. Since there is no flow through these solid boundaries, the velocity in the flow must satisfy the following conditions on its wall-normal component

$$\Im(V(x \pm ib)) = 0. \quad (3)$$

Since our model is inviscid, the tangential (slip) velocity component on the walls $\Re(V(x \pm ib))$ need not vanish. In order to satisfy condition (3), the velocity field induced by the vortex sheet, given by the RHS of the Birkhoff-Rott equation (2), must be augmented by including a suitable potential velocity field $W(z) := \frac{\partial \phi}{\partial x}(z) - i \frac{\partial \phi}{\partial y}(z)$ expressed in terms of a potential ϕ . This potential is constructed to cancel the normal component of the velocity induced by the vortex sheet on the boundary $y = \pm b$, such that the modified Birkhoff-Rott equation takes the

following form

$$\begin{aligned}\frac{\partial z^*}{\partial t}(\gamma, t) &= V(z(\gamma, t)) + W(z(\gamma, t)) \\ &= \frac{1}{4\pi i} \text{pv} \int_0^{2\pi} \cot\left(\frac{z(\gamma, t) - z(\gamma', t)}{2}\right) d\gamma' \\ &\quad + \frac{\partial \phi}{\partial x}(z(\gamma, t)) - i \frac{\partial \phi}{\partial y}(z(\gamma, t)), \quad \gamma \in [0, 2\pi], \quad t > 0,\end{aligned}\tag{4a}$$

$$\left(\frac{\partial^2}{\partial x^2} + \frac{\partial^2}{\partial y^2}\right)\phi = 0 \quad \text{in } \Omega,\tag{4b}$$

$$\phi(x, y) = \phi(x + 2\pi, y), \quad x \in (0, 2\pi), \quad -b < y < b,\tag{4c}$$

$$\frac{\partial \phi}{\partial y}\Big|_{y=\pm b} = \Im \left[\frac{1}{4\pi i} \int_0^{2\pi} \cot\left(\frac{x \pm ib - z(\gamma', t)}{2}\right) d\gamma' \right], \quad x \in (0, 2\pi),\tag{4d}$$

where relations (4c)–(4d) are the boundary conditions for the Laplace equation (4b) defining the potential ϕ . We emphasize that the potential depends linearly on the velocity induced by the vortex sheet on the solid boundaries $y = \pm b$, cf. (4d). Equation (2) and system (4) are complemented with a suitable initial condition $z(\gamma, 0) = z_0(\gamma)$, $\gamma \in [0, 2\pi]$. As can be readily verified, they admit an equilibrium solution (a fixed point) $\tilde{z}(\gamma, t) := \gamma$ for $\gamma \in [0, 2\pi]$, i.e., $\frac{\partial}{\partial t}\tilde{z}^*(\gamma, t) = 0$, which corresponds to a flat (undeformed) sheet, cf. Figure 1. The stability of this equilibrium solution, and in particular how it depends on the parameter b defining confinement, is the main question addressed in this paper.

We note that since the sheet intensity, which is assumed constant and equal to unity, represents the difference between the tangential velocity components on both sides of the sheet, the horizontal velocity component in the flow is defined up to an arbitrary constant u_0 which, however, does not affect the stability properties of the sheet. To see this, we perform a change of coordinates to a moving frame of reference $Z(t, \gamma) := z(t, \gamma) - u_0 t$, such that equation (4a) becomes $\frac{\partial Z^*}{\partial t}(\gamma, t) = V(Z(\gamma, t) + u_0 t) + W(Z(\gamma, t) + u_0 t) - u_0$. It is now clear that the Jacobian of the RHS of this equation, and hence also the stability properties of the sheet, do not depend on the constant term u_0 . Therefore, without loss of generality, below we will assume that $u_0 = 0$. The stability of confined equilibria described by system (4) is studied in the next section.

3 Stability Analysis

In this section we first review the stability properties of unconfined sheet equilibria governed by the Birkhoff-Rott equation (2), which are classical results [15, 16], and then proceed to analyze the stability of confined sheet equilibria described by system (4). As a starting point, we perturb the equilibrium state infinitesimally as

$$z(\gamma, t) = x + \varepsilon \zeta(\gamma, t),\tag{5}$$

for some $0 < \varepsilon \ll 1$. Here, $\zeta(\gamma, t)$ is a perturbation represented in the periodic setting, cf. (1), as

$$\zeta(\gamma, t) = \sum_{k=-\infty}^{\infty} \hat{\zeta}_k(t) e^{ik\gamma},\tag{6}$$

in which $\hat{\zeta}_k \in \mathbb{C}$, $k \in \mathbb{Z}$, are the Fourier coefficients. Then, we obtain the linearized equation for the evolution of the perturbation $\zeta(\gamma, t)$ as follows [16]

$$\begin{aligned}
\frac{\partial \zeta^*}{\partial t}(\gamma, t) &= V'[\zeta](\gamma, t) := -\frac{1}{8\pi i} \text{pv} \int_0^{2\pi} \frac{\zeta(\gamma, t) - \zeta(\gamma', t)}{\sin^2\left(\frac{\gamma - \gamma'}{2}\right)} d\gamma' \\
&= \sum_{k=-\infty}^{\infty} \hat{\zeta}_k(t) e^{ik\gamma} \left[-\frac{1}{8\pi i} \text{pv} \int_0^{2\pi} \frac{1 - e^{-ik\gamma'}}{\sin^2\left(\frac{\gamma'}{2}\right)} d\gamma' \right] \\
&= -\frac{1}{2i} \sum_{k=1}^{\infty} k \hat{\zeta}_k(t) e^{ik\gamma} - \frac{1}{2i} \sum_{k=1}^{\infty} k \hat{\zeta}_{-k}(t) e^{-ik\gamma},
\end{aligned} \tag{7}$$

where $V'[\zeta]$ is a linear operator acting on ζ obtained as the linearization of the RHS of equation (2) around the equilibrium configuration. Since

$$\frac{\partial \zeta^*}{\partial t} = \sum_{k=-\infty}^{\infty} \frac{d\hat{\zeta}_k^*}{dt} e^{-ik\gamma} = \sum_{k=1}^{\infty} \frac{d\hat{\zeta}_k^*}{dt} e^{-ik\gamma} + \sum_{k=1}^{\infty} \frac{d\hat{\zeta}_{-k}^*}{dt} e^{ik\gamma} + \frac{d\hat{\zeta}_0}{dt}, \tag{8}$$

equating coefficients of the Fourier components in (7) and (8) corresponding to different wavenumbers k , we obtain an infinite system of linear ordinary differential equations (ODEs) for the evolution of the coefficients $\hat{\zeta}_k$ in a block-diagonal form

$$\frac{d\hat{\zeta}_0}{dt} = 0, \tag{9a}$$

$$\frac{d}{dt} \begin{bmatrix} \hat{\zeta}_k \\ \hat{\zeta}_{-k}^* \end{bmatrix} = \frac{ik}{2} \begin{bmatrix} 0 & -1 \\ 1 & 0 \end{bmatrix} \begin{bmatrix} \hat{\zeta}_k \\ \hat{\zeta}_{-k}^* \end{bmatrix} =: \mathbf{A}_k \begin{bmatrix} \hat{\zeta}_k \\ \hat{\zeta}_{-k}^* \end{bmatrix}, \quad k = 1, 2, \dots \tag{9b}$$

corresponding to the original continuous integro-differential problem. Since this latter system has a block-diagonal structure, key insights about the infinite-dimensional problem can be obtained by analyzing just a single block, independently from all other blocks. The eigenvalues corresponding to each diagonal block with matrix \mathbf{A}_k , $k \geq 1$, cf. (9b), are $\lambda_k = \pm \frac{k}{2}$. Thus, we see that at each wavenumber k there is an unstable and stable mode and the growth rate of the former is proportional to the wavenumber k , such that small-scale perturbations always become more unstable. This extreme form of instability underlies the ill-posedness of the initial-value problem for the Birkhoff-Rott equation [4].

We now go on to analyze the stability of equilibria of confined vortex sheets governed by system (4) whose linearization takes the form

$$\frac{\partial \zeta^*}{\partial t}(\gamma, t) = V'[\zeta](\gamma, t) + W'[\zeta](\gamma, t) \tag{10}$$

in which $W'[\zeta](\gamma) = \frac{\partial \phi'}{\partial x}(\gamma, y=0) - i \frac{\partial \phi'}{\partial y}(\gamma, y=0)$ represents the linearization of the potential velocity W in (4a) around the equilibrium. At every instant of time t the linearized potential

ϕ' solves the problem

$$\left(\frac{\partial^2}{\partial x^2} + \frac{\partial^2}{\partial y^2}\right) \phi' = 0 \quad \text{in } \Omega, \quad (11a)$$

$$\phi'(x, y) = \phi'(x + 2\pi, y), \quad x \in (0, 2\pi), \quad -b < y < b, \quad (11b)$$

$$\left.\frac{\partial \phi'}{\partial y}\right|_{y=\pm b} = \Im [V'[\zeta](x \pm ib, t)], \quad x \in (0, 2\pi), \quad (11c)$$

where

$$V'[\zeta](x \pm ib, t) = \frac{1}{8\pi i} \int_0^{2\pi} \frac{\zeta(\gamma', t) d\gamma'}{\sin^2\left(\frac{x \pm ib - \gamma'}{2}\right)}. \quad (12)$$

Noting (6) and the fact that $V'[\zeta]$ is linear in the perturbation ζ , the RHS in the boundary condition (11c) can be expressed as

$$\Im [V'[\zeta](x \pm ib, t)] = \Im \left[\frac{1}{8\pi i} \sum_{k=-\infty}^{\infty} \widehat{\zeta}_k(t) I_k(x \pm ib) \right], \quad (13)$$

$$\text{where } I_k(x \pm ib) := \int_0^{2\pi} \frac{e^{ik\gamma'} d\gamma'}{\sin^2\left(\frac{x \pm ib - \gamma'}{2}\right)}, \quad k \in \mathbb{Z}, \quad (14)$$

represents the linearized complex velocity induced by the Fourier component of the perturbation ζ with wavenumber k , cf. (6), on the solid boundaries.

Our goal is to eliminate the linearized potential ϕ' such that the term $W'[\zeta]$ in (10) can be expressed explicitly as a function of the perturbation ζ , which in turn will allow us to assess the effect of the confinement on the stability of the equilibrium \tilde{z} . This will be done in three simple steps described in the following three sections.

3.1 Evaluation of integrals I_k in (14)

The integrals I_k , $k \in \mathbb{Z}$, are defined in the classical (Riemann) sense (i.e., they are nonsingular) and will be evaluated using the calculus of residues. To this end, we map the integral (14) to the positively oriented unit circle $|z| = 1$ on the complex plane \mathbb{C} using the change of variables $z = e^{i\gamma}$, such that $dz = iz d\gamma$ and (14) becomes

$$I_k(\xi) = 4i \oint_{|z|=1} \frac{z^k dz}{e^{i\xi} - 2z + e^{-i\xi} z^2} = 4i e^{i\xi} \oint_{|z|=1} \frac{z^k dz}{(z - e^{i\xi})^2}, \quad \text{where } \xi := x \pm ib. \quad (15)$$

In order to evaluate the integral in (15) using the calculus of residues, we decompose its integrand expression into partial fractions, noting that k can take both positive and negative values,

$$\frac{z^k}{(z - e^{i\xi})^2} = \frac{A_1}{z} + \dots + \frac{A_{|k|}}{z^k} + \frac{B_1}{z - e^{i\xi}} + \frac{B_2}{(z - e^{i\xi})^2} + C_0 + C_1 z + \dots + C_{|k|-2} z^{|k|-2}, \quad (16)$$

where $A_1, \dots, A_{|k|}, B_1, B_2, C_0, C_1, \dots, C_{|k|-2} \in \mathbb{C}$, such that

$$\oint_{|z|=1} \frac{z^k dz}{(z - e^{i\xi})^2} = 2\pi i [A_1 + B_1].$$

We note that $A_1 = \dots = A_{|k|} = 0$ if $k \geq 0$ and $C_0 = C_1 = \dots = C_{|k|-2} = 0$ if $k \leq 0$. We then have the following four cases depending on the signs of k and $y = \Im(\xi) = \pm b$:

- $k \geq 0$ and $y = b > 0$ ($|e^{i\xi}| < 1$), such that $A_1 = 0$, $B_1 = ke^{(k-1)i\xi}$ and

$$\oint_{|z|=1} \frac{z^k dz}{(z - e^{i\xi})^2} = 2\pi i \left[ke^{(k-1)i\xi} \right],$$

- $k \geq 0$ and $y = -b < 0$ ($|e^{i\xi}| > 1$), such that $A_1 = B_1 = 0$, and

$$\oint_{|z|=1} \frac{z^k dz}{(z - e^{i\xi})^2} = 0,$$

- $k < 0$ and $y = b > 0$ ($|e^{i\xi}| < 1$), such that $A_1 = -B_1 = -ke^{(k-1)i\xi}$, $A_1 + B_1 = 0$, and

$$\oint_{|z|=1} \frac{z^k dz}{(z - e^{i\xi})^2} = 0,$$

- $k < 0$ and $y = -b < 0$ ($|e^{i\xi}| > 1$), such that $A_1 = -ke^{(k-1)i\xi}$, $B_1 = 0$ and

$$\oint_{|z|=1} \frac{z^k dz}{(z - e^{i\xi})^2} = -2\pi i \left[ke^{(k-1)i\xi} \right].$$

Thus, we finally obtain

$$I_k(\xi) = \begin{cases} -8\pi ke^{ik\xi}, & k \geq 0 \text{ and } \Im(\xi) > 0 \\ +8\pi ke^{ik\xi}, & k < 0 \text{ and } \Im(\xi) < 0, \\ 0, & \text{otherwise} \end{cases} \quad (17)$$

a result which can be verified by approximating integrals (15) numerically.

3.2 Solution of System (11) for Linearized Potential

Given the linearity of (11a) and the form of the boundary condition in (11c), which involves a superposition of Fourier components with different wavenumbers k , we represent the perturbation potential in the form of a series

$$\phi'(x, y) = \sum_{k=0}^{\infty} \phi'_k(x, y), \quad \text{where} \quad \phi'_k(x, y) := \frac{1}{2} ke^{-kb} \left[P_k(y) e^{ikx} + P_k^*(y) e^{-ikx} \right] \quad (18)$$

for some functions $P_k : [-b, b] \rightarrow \mathbb{C}$, $k = 0, 1, \dots$. Using formulas (17) and representation (18), the boundary condition (11c) becomes equivalent to the following set of relations

$$\left. \frac{\partial \phi'_k}{\partial y} \right|_{y=b} = \Im \left[ik \hat{\zeta}_k e^{-kb} e^{ikx} \right] = \frac{ke^{-kb}}{2} \left(\hat{\zeta}_k e^{ikx} + \hat{\zeta}_k^* e^{-ikx} \right), \quad (19a)$$

$$\left. \frac{\partial \phi'_k}{\partial y} \right|_{y=-b} = \Im \left[ik \hat{\zeta}_{-k} e^{-kb} e^{-ikx} \right] = \frac{ke^{-kb}}{2} \left(\hat{\zeta}_{-k} e^{-ikx} + \hat{\zeta}_{-k}^* e^{ikx} \right), \quad k \geq 0, \quad (19b)$$

such that system (11) reduces to a family of 1D boundary-value problems

$$\frac{d^2}{dy^2} P_k(y) - k^2 P_k(y) = 0, \quad \text{in } (-b, b), \quad k = 0, 1, 2, \dots, \quad (20a)$$

$$\frac{d}{dy} P_k(b) = \hat{\zeta}_k, \quad \frac{d}{dy} P_k(-b) = \hat{\zeta}_{-k}^*. \quad (20b)$$

Their solutions are, noting that $\hat{\zeta}_0 \equiv 0$,

$$P_0(y) = 0, \quad (21a)$$

$$P_k(y) = \left(\hat{\zeta}_k - \hat{\zeta}_{-k}^* \right) \frac{\cosh(ky)}{2k \sinh(kb)} + \left(\hat{\zeta}_k + \hat{\zeta}_{-k}^* \right) \frac{\sinh(ky)}{2k \cosh(kb)}, \quad k \geq 1, \quad (21b)$$

such that the perturbation potential finally becomes

$$\begin{aligned} \phi'(x, y) = \sum_{k=1}^{\infty} \frac{k e^{-kb}}{2} \left\{ \left[\left(\hat{\zeta}_k - \hat{\zeta}_{-k}^* \right) \frac{\cosh(ky)}{2k \sinh(kb)} + \left(\hat{\zeta}_k + \hat{\zeta}_{-k}^* \right) \frac{\sinh(ky)}{2k \cosh(kb)} \right] e^{ikx} \right. \\ \left. + \left[\left(\hat{\zeta}_k^* - \hat{\zeta}_{-k} \right) \frac{\cosh(ky)}{2k \sinh(kb)} + \left(\hat{\zeta}_k^* + \hat{\zeta}_{-k} \right) \frac{\sinh(ky)}{2k \cosh(kb)} \right] e^{-ikx} \right\}. \end{aligned} \quad (22)$$

3.3 Stability of Modified System (4)

In order to evaluate the term $W'[\zeta](\gamma, t)$ in (10), we need to compute the partial derivatives of the perturbation potential (22) at the location of the unperturbed sheet \tilde{z} , i.e., at $y = 0$,

$$\left. \frac{\partial \phi'}{\partial x} \right|_{y=0} = \frac{1}{2} \sum_{k=1}^{\infty} k e^{-kb} \left[ik P_k(0) e^{ikx} - ik P_k^*(0) e^{-ikx} \right], \quad (23a)$$

$$\left. \frac{\partial \phi'}{\partial y} \right|_{y=0} = \frac{1}{2} \sum_{k=1}^{\infty} k e^{-kb} \left[\frac{d}{dy} P_k(0) e^{ikx} + \frac{d}{dy} P_k^*(0) e^{-ikx} \right]. \quad (23b)$$

Using (21) and recognizing that under the assumption of unit sheet strength at equilibrium we have $\gamma = x$, the following expression is obtained

$$W'[\zeta](\gamma, t) = \frac{i}{2} \sum_{k=1}^{\infty} \frac{k e^{-kb}}{\sinh(2kb)} \left[\left(e^{-kb} \hat{\zeta}_k - e^{kb} \hat{\zeta}_{-k}^* \right) e^{ik\gamma} - \left(e^{kb} \hat{\zeta}_k^* - e^{-kb} \hat{\zeta}_{-k} \right) e^{-ik\gamma} \right]. \quad (24)$$

Inserting this expression into (10) and rewriting this equation in terms of Fourier components as was done earlier for the original problem (9), we obtain an infinite system of ODEs for the Fourier coefficients preserving the block-diagonal structure of the original problem, with the block corresponding to the wavenumber k given by

$$\frac{d \hat{\zeta}_0}{dt} = 0, \quad (25a)$$

$$\begin{aligned} \frac{d}{dt} \begin{bmatrix} \hat{\zeta}_k \\ \hat{\zeta}_{-k}^* \end{bmatrix} &= \frac{ik}{2} \begin{bmatrix} f_k(b) & -(1 + g_k(b)) \\ (1 + g_k(b)) & -f_k(b) \end{bmatrix} \begin{bmatrix} \hat{\zeta}_k \\ \hat{\zeta}_{-k}^* \end{bmatrix} \\ &= \frac{ik}{2} \begin{bmatrix} \text{csch}(2kb) & -\coth(2kb) \\ \coth(2kb) & -\text{csch}(2kb) \end{bmatrix} \begin{bmatrix} \hat{\zeta}_k \\ \hat{\zeta}_{-k}^* \end{bmatrix} =: \tilde{\mathbf{A}}_k \begin{bmatrix} \hat{\zeta}_k \\ \hat{\zeta}_{-k}^* \end{bmatrix}, \quad k = 1, 2, \dots, \end{aligned} \quad (25b)$$

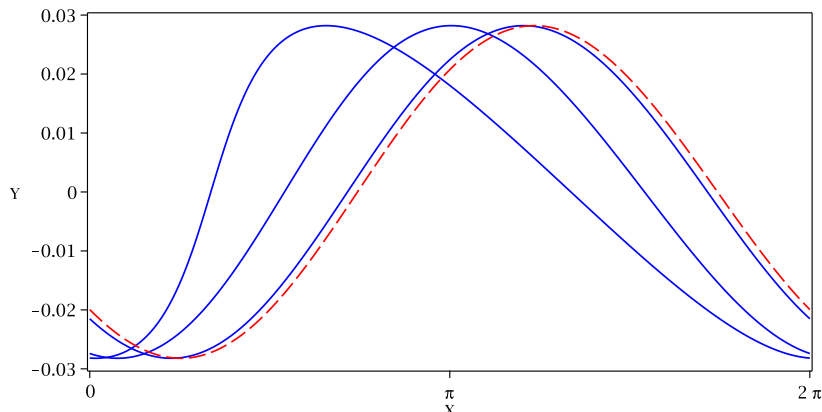


Figure 2: Equilibria deformed as $\tilde{z} + \epsilon u_1$ with the unstable eigenvectors u_1 of (red dashed line) the unconfined problem (9) and (blue solid lines) the confined problem (25) with $b = 0.05, 0.25, 1.25$ (more deformed sheets correspond to smaller values of b). In all cases we have $k = 1$ and $\epsilon = 0.05$, whereas the eigenvectors are normalized such that $\int_0^{2\pi} [\Im(u_1(\gamma'))]^2 d\gamma' = 1$ which ensures the same mean-square transverse displacement in all cases, thereby making it easier to compare the deformations corresponding to different values of b . The deformed equilibria are shifted by an appropriate distance in the horizontal direction so that their horizontal extent is $[0, 2\pi]$ in all cases.

where the expressions

$$f_k(b) := \frac{1}{\sinh(2kb)}, \quad (26a)$$

$$g_k(b) := \frac{e^{-2kb}}{\sinh(2kb)} \quad (26b)$$

represent “corrections” due to confinement effects.

Since when $k > 0$ we have $\lim_{b \rightarrow 0} f_k(b), g_k(b) = \infty$ and $\lim_{b \rightarrow \infty} f_k(b), g_k(b) = 0$, the terms representing the effect of confinement in matrix $\tilde{\mathbf{A}}_k$ vanish when the distance b increases such that, as expected, the unconfined case is recovered in the limit $b \rightarrow \infty$. On the other hand, these terms become dominant as the solid walls approach the vortex sheet. However, the eigenvalues of matrix $\tilde{\mathbf{A}}_k$ do not depend on the distance b . They are given by $\tilde{\lambda}_k = \pm \frac{k}{2}$ and are identical to the eigenvalues of matrix \mathbf{A}_k , cf. (9b), describing the linearized evolution of unconfined vortex sheets. Thus, interestingly, within the inviscid model considered here, confinement has no effect on the growth rates of the unstable modes.

We now consider how confinement affects the form of unstable eigenmodes and sheet equilibria deformed as $\tilde{z} + \epsilon u_1$ by the unstable modes u_1 with wavenumber $k = 1$ are shown in Figure 2 for different values of parameter b . Because the perturbation amplitude $\epsilon = 0.05$ is relatively small, the deformed equilibrium in the unconfined case resembles a slanted sine wave (although the slant is imperceptibly small due to the vertical scale in Figure 2 being magnified with respect to the horizontal scale). Since functions $f_k(b)$ and $g_k(b)$, cf. (26a)–(26b), vanish very rapidly as b increases, differences between the unstable modes in the unconfined and confined cases are significant only for very small values of b , of order $\mathcal{O}(10^{-1})$ or less,

and are essentially imperceptible when b is $\mathcal{O}(1)$ or larger, which is the more relevant case from the practical point of view. The effect of the confinement is to steepen the profile of the unstable modes, such that the eigenmodes with the same wavenumber k become increasingly non-normal as b decreases. The influence of the confinement on the growth of instabilities in the nonlinear regime is explored using numerical computations in the next section.

4 Nonlinear Growth of Instabilities

In this section we solve system (4) numerically for different values of the parameter b in order to characterize the growth of instabilities beyond the linear regime discussed in Section 3. System (4) is discretized in space using the collocation approach devised in [16], but without regularization, on a mesh consisting of $N = 128$ equispaced grid points, see also [11]. The normal velocity component on the channel boundaries is evaluated by approximating the integral in (4d) with the trapezoidal quadrature (which is spectrally accurate for smooth functions defined on periodic domains). After computing the discrete Fourier transform of this quantity, the velocity components due to potential ϕ are determined analytically as described in Section 3, cf. (18)–(23), with the difference that they are now evaluated at the actual sheet location $z(\gamma, t)$ rather than on the line $y = 0$. Given the ill-posedness of the Birkhoff-Rott equation resulting in its extreme sensitivity to round-off errors, all calculations are performed with increased arithmetic precision, typically using 64 significant digits, which is done using **Advanpix**, a Multiprecision Computing toolbox for MATLAB [17]. The resulting ODE system is integrated in time using a multiprecision version of the routine **ode45**. The relative and absolute tolerance are both set to 10^{-8} which in the course of extensive tests was found to ensure converged results. We note that with sufficient arithmetic precision there is no need to use the spectral-filtering technique introduced by [7] to control the spurious growth of round-off errors.

We use the same initial condition as originally employed in [7], i.e., $z_0(\gamma) = \gamma + 2\pi\epsilon_0(1 - i)\sin\gamma$, $\gamma \in [0, 2\pi]$, where $\epsilon_0 = 0.01$, which represents the equilibrium configuration perturbed with the unstable eigenmode of the unconfined problem with wavenumber $k = 1$ (because of how our domain is defined, this initial condition is scaled by a factor of 2π as compared to [7]). We emphasize that since in the absence of regularization the Birkhoff-Rott system (2) develops a curvature singularity in finite time [4, 7, 10], our computations in the nonlinear regime can be carried out for relatively short times only when the solution remains well resolved.

In order to characterize the evolution of perturbations in the linear and nonlinear regime we define the following two quantities

$$E_0(t) := \epsilon_0^2 \int_0^{2\pi} |\zeta(\gamma, t)|^2 d\gamma, \quad (27a)$$

$$E(t) := \int_0^{2\pi} |z(\gamma, t) - \gamma|^2 d\gamma. \quad (27b)$$

We note that these quantities represent the sum of the “energy” associated with the transverse displacement of the sheet and its longitudinal deformation, the latter of which is related to the perturbation of the initially uniform circulation density of the sheet. Since in all cases quantities (27a)–(27b) evolve in a similar way, in Figure 3 we show their difference $E(t) - E_0(t)$ as a function of time t for different values of b . We see that as b decreases the difference between

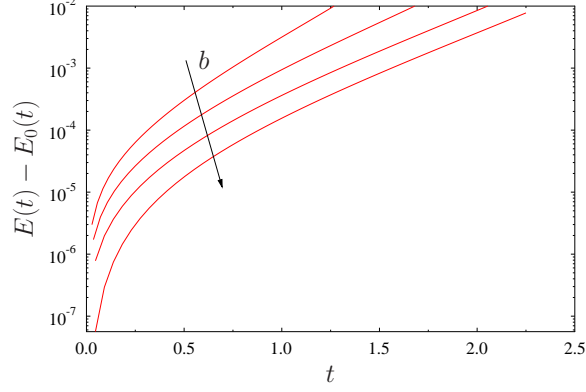


Figure 3: The difference $E(t) - E_0(t)$ between the perturbation energy in the nonlinear and linear evolution, cf. (27a)–(27b), as a function of time t for $b = 0.25, 0.5, 1, 10$. The arrow indicates the trend with the increase of b .

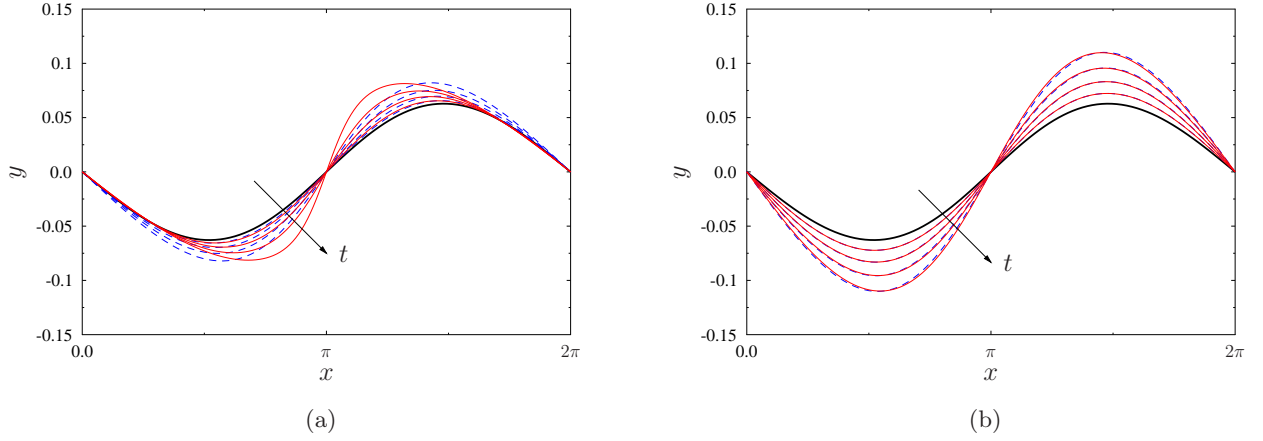


Figure 4: Solutions of (a) the confined problem with $b = 0.25$ and (b) the unconfined problems at five equispaced time levels in the interval $[0, 1.375]$. Dashed blue lines and solid red lines represent solutions of the nonlinear and linear problem (4) and (10)–(12), respectively, whereas the thick black line corresponds to the initial condition z_0 . The arrows indicate the trend with the increase of time t .

the nonlinear and linear evolution becomes more significant. The case corresponding to $b = 10$, which is the largest value of this parameter we considered, is essentially indistinguishable from the unconfined case. On the other hand, for smaller values of b the curvature singularity tends to occur earlier, so the nonlinear evolution can only be computed for shorter times in these cases.

Solutions to the nonlinear and linear system (4) and (10)–(12) obtained for $b = 0.25$ are shown at different times in the physical space in Figure 4(a). We note that in this case with significant confinement the perturbation amplitude $2\pi \cdot 0.01$ represents about 25% of the channel half-width. For comparison, in Figure 4(b) we show the corresponding solutions of the unconfined problems obtained at the same time levels. As is evident from these two figures, the primary effect of the confinement is to increase the “steepness” of the perturbed sheet while its transverse displacement is reduced with respect to the unconfined case.

5 Conclusions

We have proposed a simple model for the evolution of an inviscid vortex sheet in a potential flow in a confined geometry representing a channel with parallel walls. It is obtained by augmenting the standard Birkhoff-Rott equation with a potential field representing the effect of the solid boundaries. Next we considered the stability of equilibria corresponding to flat sheets and demonstrated through analytical computations that the presence of the solid boundaries does not affect the block-diagonal structure of the modified Birkhoff-Rott equation linearized around the equilibrium and, more importantly, the growth rates of the unstable modes remain unchanged with respect to the case with no confinement. Thus, in the presence of solid boundaries the equilibrium solution of the Birkhoff-Rott equation retains its extreme form of instability with the growth rates of the unstable modes increasing in proportion to their wavenumbers. We note that this finding is in fact also implied by Rayleigh’s classical analysis of the stability of parallel flows [13, 14] as well as by the results reported in [1], although this observation does not appear to have been explicitly stated before. As an implication of this finding, we conclude that also in the presence of confinement the Birkhoff-Rott equation cannot be integrated numerically past the Moore singularity [4] into the roll-up regime unless some form of regularization is applied. Short-time numerical integration of nonlinear system (4) carried out utilizing arbitrary precision arithmetics to control round-off errors indicates that confinement enhances the growth of perturbations in the nonlinear regime which is manifested by increased deformation of the perturbed sheet, cf. Figures 3 and 4.

The physical validity of the findings reported above is certainly restricted by the assumptions inherent in our highly-idealized model, most importantly, the assumption that the flow is irrotational away from the vortex sheet. Due to boundary-layer effects, this assumption is definitely not going to be satisfied for small values of the distance b . As regards the dynamics of the vortex sheet itself, viscous effects can be accounted for using the “vortex-blob” regularization approach [5] or with the more recently proposed Euler-alpha strategy [6]. The present study lays the groundwork for performing the stability analysis of such regularized models in the presence of confinement, with a view towards designing suitable control strategies based on these models (we emphasize here that earlier stability analyses of the vortex-sheet problem [13, 14] do not in fact lend themselves to such extensions).

Acknowledgments

The author was supported through an NSERC (Canada) Discovery Grant. He also acknowledges illuminating discussions about the Birkhoff-Rott equation with Prof. Takashi Sakajo. Anonymous referees provided valuable comments on this work, in particular, regarding the connection to Rayleigh’s classical analysis.

References

- [1] T. Funada and D. D. Joseph. Viscous potential flow analysis of Kelvin-Helmholtz instability in a channel. *Journal of Fluid Mechanics*, 445:263–283, 2001.
- [2] Mukesh Kumar Awasthi, Rishi Asthana, and G.S. Agrawal. Viscous correction for the viscous potential flow analysis of Kelvin-Helmholtz instability of cylindrical flow with heat and mass transfer. *International Journal of Heat and Mass Transfer*, 78:251 – 259, 2014.
- [3] P. G. Saffman. *Vortex Dynamics*. Cambridge Monographs on Mechanics and Applied Mathematics. Cambridge University Press, Cambridge, 1992.
- [4] D. W. Moore. The spontaneous appearance of a singularity in the shape of an evolving vortex sheet. *Proc. Roy. Soc. A*, 365:105–119, 1979.
- [5] Robert Krasny. Desingularization of periodic vortex sheet roll-up. *Journal Computational Physics*, 65:292–313, 1986.
- [6] D. D. Holm, M. Nitsche, and V. Putkaradze. Euler-alpha and vortex blob regularization of vortex filament and vortex sheet motion. *Journal of Fluid Mechanics*, 555:149–176, 2006.
- [7] Robert Krasny. A study of singularity formation in a vortex sheet by the point vortex approximation. *Journal of Fluid Mechanics*, 167:65–933, 1986.
- [8] R. E. Caflisch, editor. *Mathematical Aspects of Vortex Dynamics*. SIAM, 1989.
- [9] A. J. Majda and A. L. Bertozzi. *Vorticity and Incompressible Flow*. Cambridge University Press, 2002.
- [10] A. C. DeVoria and K. Mohseni. Vortex sheet roll-up revisited. *Journal of Fluid Mechanics*, 855:299–321, 2018.
- [11] Bartosz Protas and Takashi Sakajo. Harnessing the Kelvin-Helmholtz instability: feedback stabilization of an inviscid vortex sheet. *Journal of Fluid Mechanics*, 852:146–177, 2018.
- [12] Silas Alben. Flag flutter in inviscid channel flow. *Physics of Fluids*, 27(3):033603, 2015.
- [13] Lord Rayleigh. *The theory of sound*. Macmillan and co., 2nd edition, 1894.
- [14] P.G. Drazin and W.H. Reid. *Hydrodynamic stability*. Cambridge University Press, Cambridge, UK, 2th edition, 2004.

- [15] Masaru Kiya and Mikio Arie. Helmholtz instability of a vortex sheet in uniform shear flow. *The Physics of Fluids*, 22(2):378–379, 1979.
- [16] T. Sakajo and H. Okamoto. Numerical computation of vortex sheet roll-up in the back-ground shear flow. *Fluid Dynamics Research*, 17:195–212, 1996.
- [17] LLC. Advanpix. Multiprecision computing toolbox for matlab, 2017.